Ionospheric Tomography Network of Egypt: A New Receiver Network in Support of the International Heliophysical Year

**T. W. Garner · T. L. Gaussiran II · J. A. York · D. M. Munton ·
C. M. Slack III · A. M. Mahrous**

Abstract The International Heliophysical Year (IHY) 2007 is an international scientific program designed to coordinate observations of the heliosphere, the region of space from the solar surface through the solar wind and various planetary magnetospheres to the planetary upper atmospheres. A particular emphasis is given to the development of long-term international collaborations that will study the external drivers to the space environment and climate. The Ionospheric Tomography Network of Egypt (ITNE) is one such collaboration. It is a new chain of ionospheric tomography receivers that will be deployed to investigate the equatorial regions of the Earth's ionosphere. The distribution of plasma density within 20° of the magnetic equator is highly sensitive to forcing from the solar wind through a process known as the equatorial fountain. ITNE will provide new observations of the density structures associated with the equatorial fountain.

Keywords Equatorial ionosphere · Electron content · Ionospheric data

1 Introduction

The International Heliophysical Year (IHY) is an international scientific campaign to study the linked Sun-Earth system (Harrison et al. 2005). It is an ambitious campaign attempting to coordinate solar surface, solar wind, magnetospheric, ionospheric and upper atmospheric observations. In particular, it attempts to coordinate these studies across the globe. In addition to encouraging cutting-edge scientific investigations, the IHY campaign is interested in developing long-term international scientific collaboration and strengthening the scientific infrastructure outside of Europe, North America and northeastern Asia. As part of the IHY, Helwan University in Cairo, Egypt has partnered with the Applied

T. W. Garner (✉) · T. L. Gaussiran II · J. A. York · D. M. Munton · C. M. Slack III
Space and Geophysics Lab, Applied Research Laboratories, The University of Texas at Austin,
F0252, Austin, TX 78758-4423, USA
e-mail: garner@arlut.utexas.edu

A. M. Mahrous
Faculty of Science, Helwan University, Cairo, Egypt

Research Laboratories at the University of Texas in Austin (USA), the University of Alexandria in Alexandria, Egypt, and the National Research Institute of Astronomy and Geophysics in Aswan, Egypt to deploy a chain of ionospheric tomography radio receivers, known as Coherent Ionospheric Radio Receivers (CIDR).

These radio receivers observe the Doppler shift in the UHF and VHF radio signals from low-Earth-orbiting (LEO) satellites, and derive the ionospheric electron content and ionospheric-induced phase variations along the line-of-sight between the satellite and the ground receiver. When a chain of receivers are deployed along the ground track of a satellite's orbit, these electron content measurements from these receivers can be used to reconstruct the two-dimensional electron density distribution under the spacecraft. First suggested by (Austen et al. 1988), ionospheric tomography works by assuming that the ionosphere is essentially static as the satellite passes through the receiver's field-of-view (typically less than twenty minutes). Since tomography receivers measure the Doppler shifts at high rates (on the order of a Hz or faster), they take several hundred electron content measurements per satellite pass. By assuming a static ionosphere, all of the ray paths from all of the receivers in a chain can be combined. Numerous crossing ray paths make tomography possible. There are a number of different techniques for reconstructing the electron densities from ionospheric tomography, which have been discussed in greater detail by Pryse et al. (1998) and Kunitsyn and Tereshchenko (2003).

Ionospheric tomography has been successfully used to study several large-scale ionospheric structures. Many of these studies have looked at plasma structures on the order of a few hundred kilometers (or a few degrees of latitude). For example, several authors have looked at the the structure of the ionospheric trough (e.g., Pryse et al. 1996, 2006), which is a narrow region of lower plasma density on the nightside of the ionosphere between the auroral oval and the formerly sunlit ionosphere (Moffett and Quegan 1983). In addition, several studies (e.g., Coker et al. 2004; Middleton et al. 2005; Bust and Crowley 2007) have used tomography chains to observe the polar cap ionization patches, which are large-scale (several hundred kilometer) plasma structures that convect across the polar cap (Tsunoda 1988). Tomography chains have previously focused upon the high-latitude ionosphere because the polar orbits of the beacon satellites provide excellent coverage of this region. However, the usefulness of ionospheric tomography is not limited to higher latitudes, as several different studies have demonstrated. A tomography chain established in Taiwan has been used to study the behavior of the plasma density peaks produced by the equatorial fountain (e.g., Andreeva et al. 2000; Yeh et al. 2001; Franke et al. 2003). These peaks, which are typically situated between $10°$ and $25°$ magnetic latitude, are caused by a vertical $\mathbf{E} \times \mathbf{B}$ plasma drift at the magnetic equator. The plasma is pushed to higher altitudes and diffuses downward along magnetic field lines to higher latitudes (Walker 1981). Despite years of observations, the daily variability and stormtime evolution of the equatorial fountain remain outstanding problems in ionospheric physics and space weather (e.g., Lin et al. 2005a, b; Garner et al. 2006).

The Ionospheric Tomography Network in Egypt (ITNE) is being established in order to help address these vexing science problems. This new CIDR array will provide new observations of plasma structures near the ionization peaks associated with the equatorial fountain. This new chain will cover most of the length of the Egypt. More importantly, it will extend from roughly $13–24°$ magnetic latitude. Since the typically field-of-view for a CIDR receiver extends $10-15°$ to either side of receiver, ITNE's field-of-view should extend from roughly $40°$ to the magnetic equator. Hence, it will be well suited to study the plasma structures associated with the equatorial fountain. This paper provide a description of the CIDR system (Sect. 2) and the ITNE (Sect. 3) to be set up in 2008.
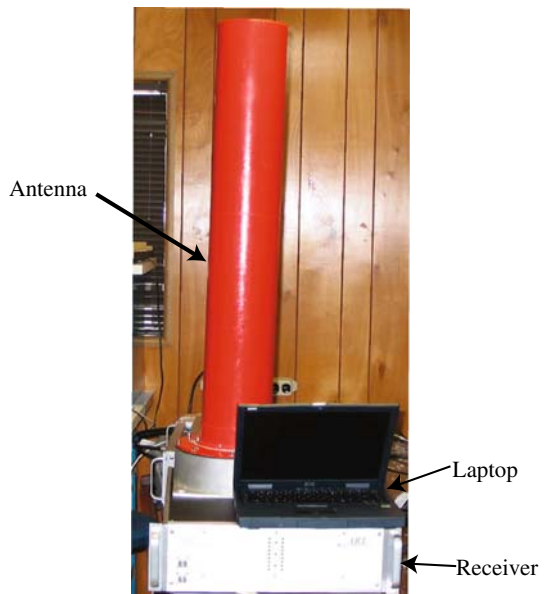
2 Coherent Ionospheric Doppler Receivers

2.1 Components

Each Coherent Ionospheric Doppler Receivers (CIDRs) system is composed of four primary components: an antenna, a receiver, a single frequency Global Positioning System (GPS) unit, and a laptop. Figure 1 is a picture of a CIDR system showing three of the main components. The GPS antenna is smaller than a typical computer mouse and is not shown in this photo. While different antenna designs have been tested, the primary CIDR antenna is a coupled, helical design. In addition, the antenna contains a preamplifier and a high-pass and bandpass filter. The antenna and electronics are contained in a fiberglass cylinder with an aluminum base. A 100 ft, low-loss cable connects the antenna to the receiver, which allows the antenna to be deployed up to five stories above the receiver. The majority of the system electronics are contained within the receiver. Here the analog signals from the antenna are digitized and the principle measurements are determined. The GPS unit, contained within the main receiver box, provides the CIDR with the Universal Time and geographic location of the CIDR. The final component is the laptop. Using a Linux operating system, the CIDR laptop is connected to the receiver by a USB cable and to the Internet by an Ethernet cable. The laptop is an essential component of the CIDR system. It acquires the satellite ephemeris via the Internet, converting the ephemeris information into specific observing jobs for the receiver, converting the receiver data into ASCII data files, providing a user interface that allows the user to monitor the CIDR and to adjust system parameters, and storing the CIDR output for several weeks.

2.2 Diagnostic CIDR Data

The CIDR system was initially designed to observe the ionospheric effects upon navigation signals from the U.S. Navy's Transit satellites (Danchik 1998). The radio beacons on these

Fig. 1 A photo of the CIDR system

Table 1 The radio frequencies observed by Coherent Ionosphere Doppler Receivers

| Radio Channel	VHF Frequency (MHz)	UHF Frequency (MHz)
Operational	149.988	399.968
Maintenance	149.97825	399.942
Geodetic	150.012	400.032

spacecraft transmit in either an operational or maintenance channel. In addition, a number of scientific research satellites (Bernhardt and Siefring 2006) carry radio beacons, which broadcast in a geodetic channel that the CIDRs observe. Each radio beacon transmits a UHF and VHF radio signal. Table 1 presents the radio frequencies for each of the three beacon modes observed by the CIDRs.

Each CIDR records the frequency Doppler shift and the phasor between the incoming broadband signal and the internal system clock for both the UHF and VHF channels. These measurements are taken at an internal data rate of 1 kHz, which can be decimated to lower frequencies specified by the user. Typically, the CIDR data is decimated to a 1 Hz data rate. The measured Doppler shift includes both the Doppler shift caused by the ionospheric time delay and the satellite motion. The satellite motions dominates the measured Doppler shift. The difference phasor measures the phase difference between the incoming signal and the expected signal, and is related to both the signal strength of the incoming signal and the phase shift of the signal within the receiver. In the raw data, the phasor values are given as a correlation count from 0 to 195.31 with pure noise equal to 97.66. In post-processing, the phasor values are normalized to values from −1 to 1. The phasor contains two components: a correlation count [CC] and a phase error [PE]. These components correspond to the amplitudes of the in-phase and quadrature terms of the correlated signal within the receiver. For a perfect, noiseless measurement, the phasor will be [195.31, 97.66] or [1, 0]. The magnitude of the phasor is a measure of the signal strength received by the CIDR. Typically, CIDRs can convert Doppler shifts with phasor magnitudes as low as 0.02 (99.61) into usable TEC measurements. The phasor also give the phase shift within the receiver ϕ_{rec}, which is equal to arctan(PE/CC).

Figure 2 is an example of the local CIDR diagnostic plot. Similar plots are created during each satellite pass, and are available on the CIDR laptop both during and after the pass. The first of the diagnostic plots (the upper panel of Fig. 2) shows the measured Doppler shifts scaled to the VHF frequency (the UHF Doppler shift is divided by 3/8). This plot is useful for detecting radio interferers. A local interferer will generate a sharp turn off of expected Doppler shift, and any measurement outside of the acceptable bounds are rejected. The second diagnostic plot shows the correlation count for each channel as a function of the time. These plots basically provide a view of the signal strength at the receiver. In many ways, they are similar to a signal-to-noise measurement. In particular, measurements with a correlation count <99 are often ignored as bad data.

2.3 Ionospheric Measurements from CIDR Parameters

The fundamental ionospheric parameters observable by CIDRs are the TEC rate of change, the relative TEC, and the ionospheric phase change in the UHF and VHF channels. However, the actual measurements are the frequency Doppler shift in the UHF and VHF radio channels. Since the Doppler shift caused by the satellite's motion dominates the measured Doppler shifts, it is necessary to remove it. This is accomplished by converting
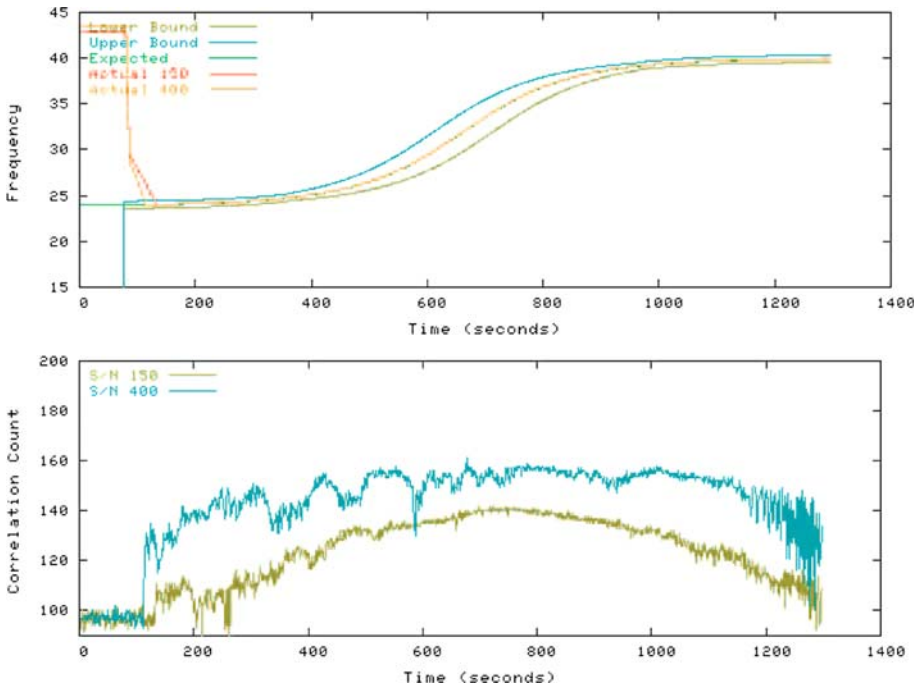
Fig. 2 A sample of the real-time CIDR diagnostic plots. The upper panel is a plot of the Doppler shifts scaled to the UHF frequency as a function of time during the satellite overpass. The measured VHF (red) and UHF (yellow) Doppler shifts are shown with expected scaled Doppler shifts (green). The side bars show the upper and lower bounds for an acceptable receiver lock. The lower panel shows the correlation count as a function time for both channels. The correlation count is unnormalized with a correlation count of 100 or greater being a usable signal (Colour online)

the measurements to a common frequency, and differencing the resultant Doppler shifts. Since the velocity induced Doppler shift is frequency independent, the frequency dependent ionospheric Doppler shift remains after the differencing. The common frequency, f_0, is roughly 50 MHz. The actual values are set at $f_0 = f_{VHF}/3 = f_{UHF}/8$. The change in the electron content, ΔT in a time step Δt is given by

$$\frac{\Delta T}{\Delta t} = \frac{e^2}{8\epsilon_0 m_e \pi^2} \frac{1}{cf_0} \frac{q_{400}^2 - q_{150}^2}{q_{400}^2 q_{150}^2} \Delta(\delta f_{dc}) \tag{1}$$

where $e = -1.602 \times 10^{-19}$ C is the electron charge, $\varepsilon_0 = 8.854 \times 10^{-12}$ F/m is the permittivity of free space, $m_e = 9.107 \times 10^{-31}$ kg is the electron mass, $c = 2.998 \times 10^8$ m/s is the speed of light in a vacuum, q is the ratio between the observed frequency and $\Delta(\delta f_{dc})$ is the difference between the down-converted Doppler shifts, which is $\Delta(\delta f_{dc}) = \delta f_{400}/8.$ $-\delta f_{150}/3$. In addition, Eq. 1 can be integrated to produce a relative TEC measurement. Figure 3 is a sample of the relative TEC observed by a CIDR located in Ancon, Peru (11.78S, 77.15W geographic; 1.2° dip latitude). In this plot, the line-of-sight TEC has been converted to a vertical TEC by dividing by the obliquity factor

$$\frac{R_e + h_{ion}}{\sqrt{(R_e + h_{ion})^2 - R_e^2 \cos^2(\theta)}} \tag{2}$$

where R_e is the Earth's radius, h_{ion} is the desired height of the ionospheric pierce point, and θ is the elevation angle of the radio ray. In this figure, the ionospheric pierce point is set at 350 km. Here, the Appleton anomaly is clearly visible, demonstrating CIDR's ability to observe spatial structures.

The ionospheric phase change at 150 MHz and 400 MHz can also be obtained from CIDR measurements. CIDRs measure the phase, ϕ_{rec}, introduced by the systems electronics in addition to measuring the Doppler shifts. Thus, the phase shift from the satellite to the antenna is given by

$$\Delta\phi = \delta f \cdot \Delta t - \phi_{rec} \qquad (3)$$

The phase change is calculated separately for each frequency, and the standard deviation of this phase change over a given time is the standard measure of the phase scintillation.

2.4 Satellite Details

The first Transit spacecraft was launched in 1959. In 1997, they were rechristened the Navy Ionospheric Monitoring Satellites (NIMS). There have been several generations of
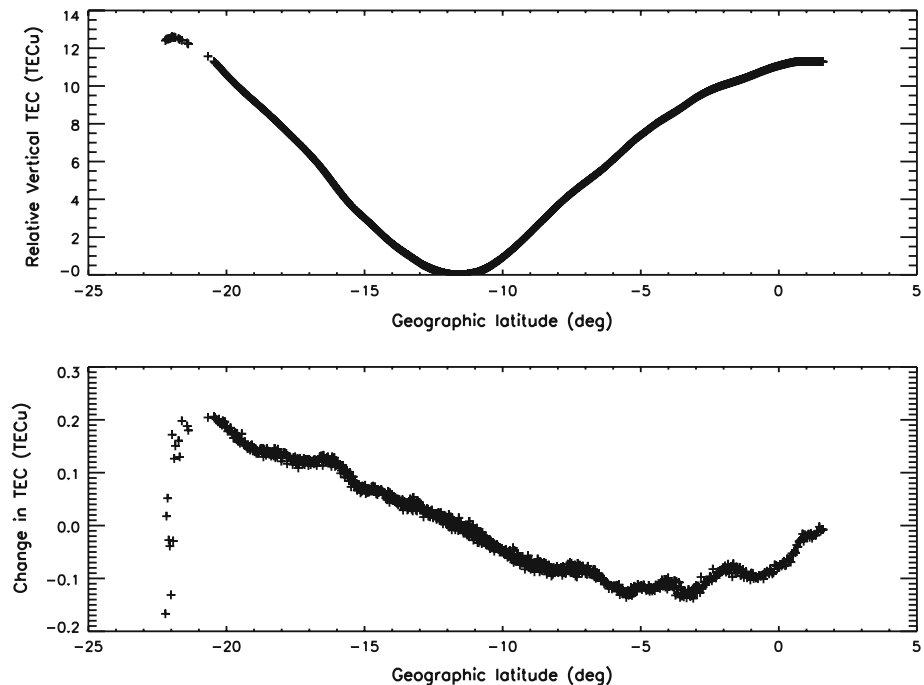
Fig. 3 A sample plot of the TEC variation associated with the equatorial fountain. These data are taken from a CIDR located in Ancon, Peru ($\sim 11°$ geographic latitude, $\sim 0°$ geomagnetic). The line-of-sight TEC has been converted to vertical and the data plotted as a function of geographic latitude. The top panels shows the relative TEC, while the bottom panel shows the change in TEC. These plots show two clear density peaks both roughly $10°$ away from the magnetic equator. ITNE will routinely observe the northern density peak. There are small scale plasma structures which are visible in the ΔTEC plot that cannot be seen in the rTEC. These features commonly occur in the data. If similar features are seen in the African sector, ITNE will be able to study them

these satellite, with the last satellite launched in 1988. They have exceeded their operational lifetime, but are still in orbit and transmitting. As these satellites gradually fail, the CIDRs increasingly rely upon the geodetic signals from new scientific satellites. These satellites (Bernhardt and Siefring 2006) operate radio beacons which are similar to the NIMS-beacons.

Low-Earth-orbit (LEO) satellites quickly pass through the CIDR field-of-view. For a typical satellite pass, the satellite moves through the receiver's field-of-view in ∼20 min. This corresponds to a ray separation of 0.15°/s. Hence, a data rate of 1 Hz is equivalent to ray paths that are 0.15° apart (assuming no ray bending). If the differences in TEC between two adjacent ray paths can be attributed to electron density variations in the F-layer between 250 and 350 km, then the TEC variations correspond to horizontal plasma structures between 654 and 916 m across. As previously noted, the maximum CIDR data rate is 1kHz, which corresponds to a ray separation of 0.54 arcsec and meter-scale F-region plasma structures.

3 Ionospheric Tomography Network of Egypt

In support of the IHY, a network of three CIDR is being deployed to Egypt. Figure 4 shows the relative position of these systems and their locations in geographic and magnetic coordinates. The northern most CIDR will be located at the University of Alexandria. The central site will be located at Helwan University in Cairo, while the southernmost CIDR will be located in Aswan at the National Research Institute of Astronomy and Geophysics. The maximum geographic longitude separation is 3.31° with ∼1.6° of separation from the central site at Helwan. This may introduce some errors into the tomographic reconstructions but these errors should be minor. The ITNE chain spans from ∼15° to ∼22° magnetic latitude. This sits right under the common location of the northern density peak

Fig. 4 A map of the Ionospheric Tomography Network of Egypt (ITNE). The squares represent the locations of the CIDRs to be deployed. The dotted lines represent the geographic latitude and longitude lines, while the dashed lines show lines of constant magnetic latitude
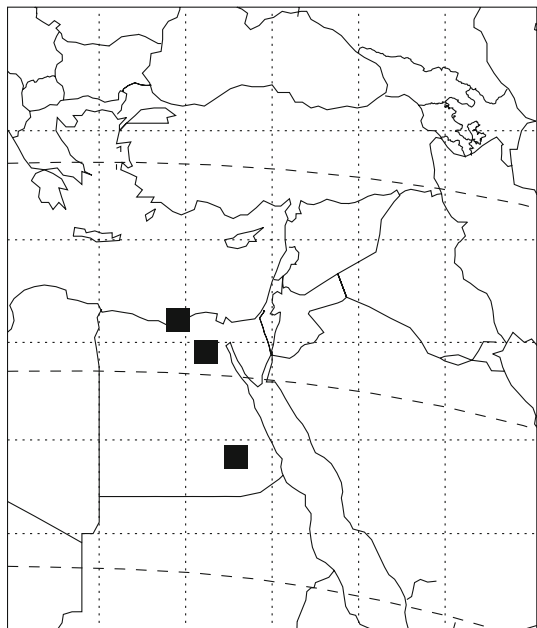
created by the equatorial fountain. ITNE should be established in December of 2007. Once a CIDR is setup, it is typically fully operational within one day. ITNE should be contributing electron content observations to the IHY program by 2008.

4 Summary

The ITNE will provide a significant contribution to the IHY program. It is well situated to observe many of the large-scale plasma structures that are associated with the equatorial fountain. Since CIDR systems operate continuously, ITNE will be able to study the daily variability of these structures as well as the stormtime evolution. Each CIDR system is capable of measuring the Doppler shift from UHF/VHF radio beacons onboard a number of different LEO satellites. From these measurements, both the relative slant electron content and the phase variations caused by the ionospheric plasma can be derived. CIDRs are highly flexible systems that operate automatically whenever a satellite is within its field-of-view. This makes them idea for deployment in the university setting as the CIDRs will be deployed in ITNE.

References

E.S. Andreeva, S.J. Franke, K.C. Yeh, Some features of the equatorial anomaly revealed by ionospheric tomography. Geophys. Res. Lett. **27**, 2465 (2000)

J.R. Austen, S.J. Franke, C.H. Liu, Ionospheric imagining using computerized tomography. Radio Sci. **23**, 299 (1988)

P.A. Bernhardt, C.L. Siefring, New satellite-based systems for ionospheric tomography and scintillation region imaging. Radio Sci. **41** (2006). doi:10.1029/2005RS003,360

G.S. Bust, G. Crowley, Tracking of polar cap ionospheric patches using data assimilation. J. Geophys. Res. **112** (2007). doi:10.1029/2005JA011597

C. Coker, G.S. Bust, R.A. Doe, T.L.Gaussiran II, High-latitude plasma structure and scintillation. Radio Sci. **39** (2004). doi:10.1029/2002RS002,833

R.J. Danchik, An overview of transit development. Johns Hopkins APL Tech. Dig. **19**, 18 (1998)

S.J. Franke, K.C. Yeh, E.S. Andreeva, V.E. Kunitsyn, A study of the equatorial anomaly ionosphere using tomographic images. Radio Sci. **38** (2003). doi:10.1029/2002RS002657

T.W. Garner, G.S. Bust, T.L. Gaussiran II, P.R. Straus, Variations in the mid-latitude and equatorial ionosphere during the October 2003 magnetic storm. Radio Sci. **41** (2006). doi:10.1029/2005RS003,399

R. Harrison, A. Breen, B. Bromage, J. Davila, 2007: International Heliophysical Year. Astron. Geophy. **46**, 3.27 (2005)

V.E. Kunitsyn, E.D. Tereshchenko, *Ionospheric Tomography* (Springer-Verlag, Berlin, 2003)

C.H. Lin, A.D. Richmond, R.A. Heelis, G.J. Bailey, G. Lu, J.Y. Liu, H.C. Yeh, S.-Y. Su, Theoretical study of the low- and midlatitude ionospheric electron density enhancment during the October 2003 superstorm: relative importance of the neutral wind and the electric field. J. Geophys. Res. **110** (2005a). doi:10.1029/2005JA011,304

C.H. Lin, A.D. Richmond, J.Y. Liu, H.C. Yeh, L.J. Paxton, G. Lu, H.F. Tsai, S.-Y. Su, Large-scale variations of the low-latitude ionosphere during the October-November 2003 superstorm: Observational results. J. Geophys. Res. **110** (2005b). doi:10.1029/2004JA010,900

H.R. Middleton, S.E. Pryse, L. Kersley, G.S. Bust, E.J. Fremouw, J.A. Secan, W.F. Denig, Evidence for the tongue of ionization under northward interplanetary magnetic field conditions. J. Geophys. Res. **110**, (2005). doi:10.1029/2004JA010800

R.J. Moffett, S. Quegan, The mid-latitude trough in the electron concentraion of the ionospheric F-layer. J. Atmos. Solar-Terr. Phys. **63**, 1285 (1983)

S.E. Pryse, L. Kersley, D.L. Rice, C.D. Russell, I.K. Walker, Tomographic imaging of the ionospheric mid-latitude trough. Ann. Geophys. **11**, 144 (1996)

S.E. Pryse, L. Kersley, C.N. Mitchell, P.S.J. Spencer, M.J. Williams, A comparison of reconstruction techniques used in ionospheric tomography. Radio Sci. **33**, 1767 (1998)

S.E. Pryse, L. Kersley, D. Malan, G.J. Bishop, Parameterization of the main ionospheric trough in the European sector. Radio Sci. **41** (2006). doi:10.1029/2005RS003364

R.T. Tsunoda, High-latitude F region irregularities: a review and synthesis. Rev. Geophys. **26**, 719 (1988)

G.O. Walker, Longitudinal structure of the F-region equatorial anomaly—a review. J. Atmos. Terr. Phys. **43**, 763 (1981)

K.C. Yeh, S.J. Franke, E.S. Andreeva, V.E. Kunitsyn, An investigation of motions of the equatorial anomaly crest. Geophys. Res. Lett. **28**, 4517 (2001)